

Yeast rRNA Expansion Segments: Folding and Function

Lizzette M. Gómez Ramos^{1,2}, Johanna M. Smeekens¹, Nicholas A. Kovacs¹,
Jessica C. Bowman¹, Roger M. Wartell³, Ronghu Wu¹ and Loren Dean Williams¹

1 - School of Chemistry and Biochemistry, Georgia Institute of Technology, 315 Ferst Drive NW, Atlanta, GA 30332-0363, USA

2 - School of Chemical and Biomolecular Engineering, Georgia Institute of Technology, 315 Ferst Drive NW, Atlanta, GA 30332-0363, USA

3 - School of Biology, Georgia Institute of Technology, 315 Ferst Drive NW, Atlanta, GA 30332-0363, USA

Correspondence to Loren Dean Williams: loren.williams@chemistry.gatech.edu

<http://dx.doi.org/10.1016/j.jmb.2016.08.008>

Edited by Daniel N. Wilson

Abstract

Divergence between prokaryotic and eukaryotic ribosomal RNA (rRNA) and among eukaryotic ribosomal RNAs is focused in expansion segments (ESs). Eukaryotic ribosomes are significantly larger than prokaryotic ribosomes partly because of their ESs. We hypothesize that larger rRNAs of complex organisms could confer increased functionality to the ribosome. Here, we characterize the binding partners of *Saccharomyces cerevisiae* expansion segment 7 (ES7), which is the largest and most variable ES of the eukaryotic large ribosomal subunit and is located at the surface of the ribosome. *In vitro* RNA-protein pull-down experiments using ES7 as a bait indicate that ES7 is a binding hub for a variety of non-ribosomal proteins essential to ribosomal function in eukaryotes. ES7-associated proteins observed here cluster into four groups based on biological process, (i) response to abiotic stimulus (e.g., response to external changes in temperature, pH, oxygen level, etc.), (ii) ribosomal large subunit biogenesis, (iii) protein transport and localization, and (iv) transcription elongation. Seven synthetases, Ala-, Arg-, Asp-, Asn-, Leu-, Lys- and TyrRS, appear to associate with ES7. Affinities of AspRS, TyrRS and LysRS for ES7 were confirmed by *in vitro* binding assays. The results suggest that ES7 in *S. cerevisiae* could play a role analogous to the multi-synthetase complex present in higher order organisms and could be important for the appropriate function of the ribosome. Thermal denaturation studies and footprinting experiments confirm that isolated ES7 is stable and maintains a near-native secondary and tertiary structure.

© 2016 Elsevier Ltd. All rights reserved.

Introduction

The core function of the ribosome is to read mRNA and synthesize coded protein. In addition, ribosomes facilitate protein folding, protein degradation, stress response and mRNA surveillance [1–3]. The increased size of ribosomal RNAs (rRNAs) in complex organisms appears to confer increased functionality to the ribosome [4]. Many auxiliary functions of large ribosomes are yet to be characterized. However, auxiliary functions correlate with rRNA size, which follows well-defined patterns:

- (i) All cytoplasmic ribosomes contain a “common core” of rRNA, which is reasonably approximated in structure by prokaryotic rRNA (Fig. 1).
- (ii) Expansion of rRNA beyond the common core is focused in a few specific regions on the ribosome called “expansion segments” (ESs) [5–9].
- (iii) ESs are located on the surface of the ribosome and are excluded from the ribosome interior and core functional centers such as the peptidyl transferase center, the decoding center, the subunit interface, and tRNA binding sites [10].

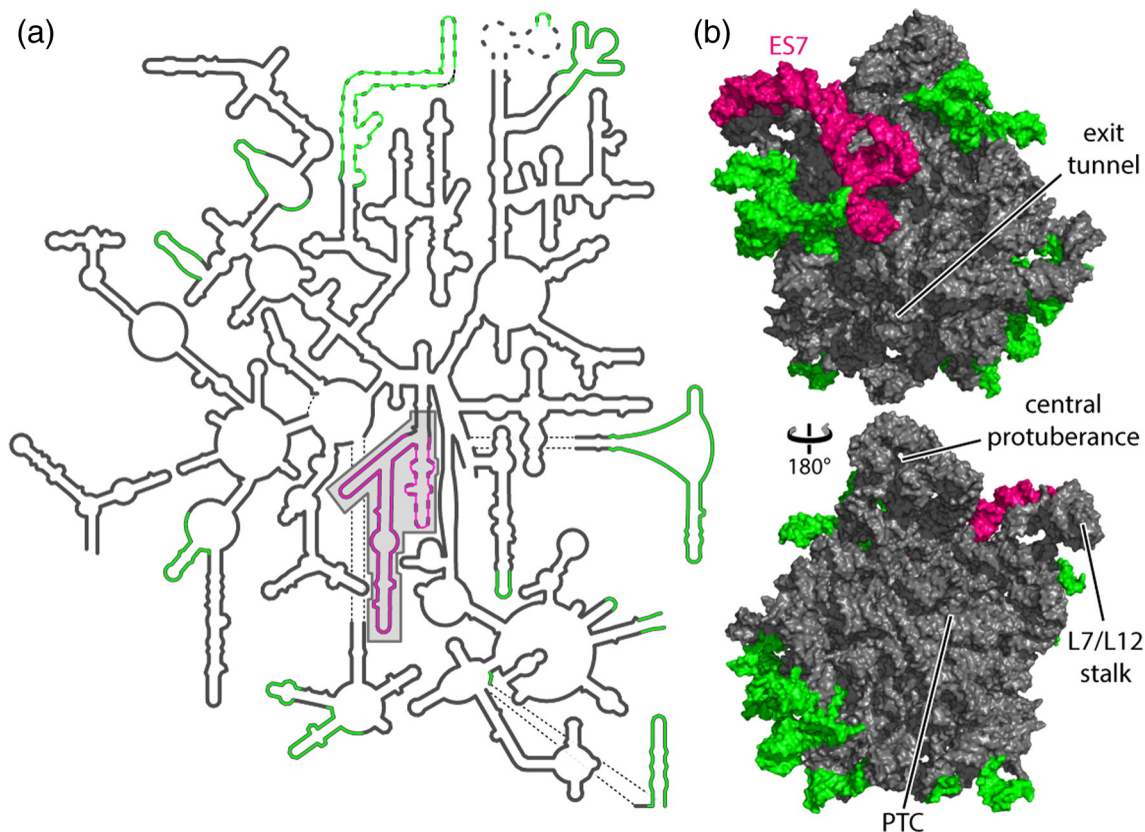


Fig. 1. The LSU rRNA of *S. cerevisiae* highlighting expansion segments. (a) Secondary structure and (b) three-dimensional structure of LSU rRNA. Common core rRNA, which is common to all cytoplasmic ribosomes, is dark gray. Expansions of *S. cerevisiae* rRNA from the common core are green, except for ES7, which is pink and is enclosed in a shaded box in panel (a). For panel (b), the top shows the back view of the LSU, and the bottom shows the front (interfacial) view. Locations of structural hallmarks such as the peptidyl transferase center (PTC), the central protuberance, stalk and tunnel exit are indicated. Thick dashed lines in panel (a) represent RNA that is not observed in the three-dimensional structure [10] and is absent in panel (b).

- (iv) Size variation is significantly greater in eukaryotes than prokaryotes and in large subunit (LSU) rRNAs than in small subunit (SSU) rRNAs [8].
- (v) rRNA size increases from bacteria/archaea to protists to metazoan and is greatest in mammals [4,9].
- (vi) rRNA size correlates with organismal complexity [4].

Here we investigate the functions of expansion segment 7 (ES7; Fig. 1) of *Saccharomyces cerevisiae*. ES7 is an extension of Helix 25 of the prokaryotic ribosome and is among the largest expansion segments of the LSU and the ribosome as a whole. ES7 is one of the most variable regions of eukaryotic rRNA. It is 210 nucleotides (nts) in *S. cerevisiae* (Fig. 2), 341 nts in *Drosophila melanogaster*, 800 nts in *Gallus gallus* and 876 nts in *Homo sapiens*. The locations of ESs on the surface of the

ribosome were established by Dervan and co-workers [11] and confirmed by three-dimensional structure determination (reviewed in Ref. [9]).

The ribosome has grown in size and complexity within certain branches of the eukaryotic tree. The LSU rRNA of *S. cerevisiae* is 3554 nts, while that of *D. melanogaster* is 4078 nts, *G. gallus* is 4725 nts and *H. sapiens* is 5227 nts. It has been proposed that ESs are involved in ribosomal regulation, packaging, turnover and biogenesis [12–14]. In trypanosomes, ESs of the small ribosomal subunit contribute to a “turret-like” structure, linking the SSU and the LSU [15]. The location of the turret suggests a role in translation initiation [16].

We characterize the secondary structure and protein binding capabilities of *S. cerevisiae* ES7. The results are consistent with a model in which expansion segments of eukaryotic ribosomes are docking sites for protein factors that are auxiliary to core ribosomal functions. These factors include aminoacyl tRNA synthetases (aaRSs), quality control proteins and chaperones.

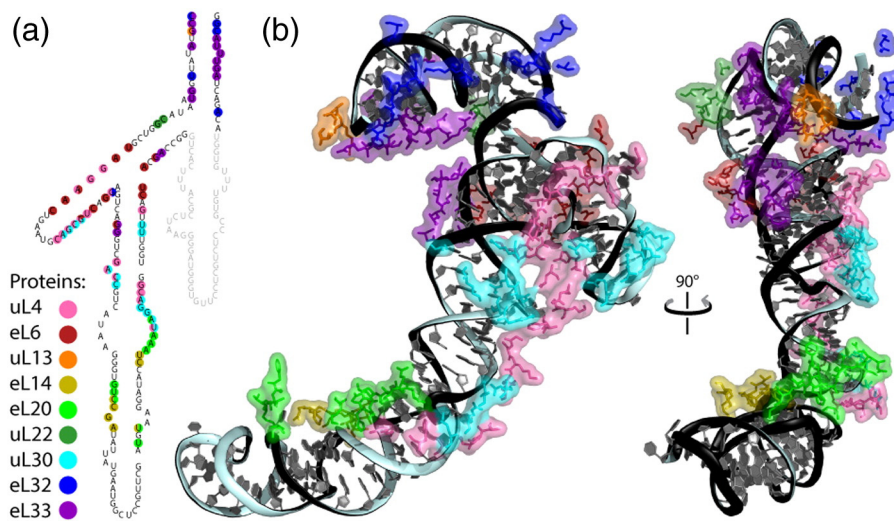


Fig. 2. ES7 rRNA interacts with ribosomal proteins in the assembled ribosome. (a) Secondary structure and (b) three-dimensional structure of *S. cerevisiae* ES7. Interactions of ribosomal proteins with ES7 are mapped onto the (a) secondary and (b) three-dimensional structures. In panel (a), nucleotides are colored by the protein with which they interact. Nucleotides not present in the three-dimensional structure are shown in gray. In panel (b), amino acids interacting with ES7 rRNA are colored by the proteins to which they belong. Coordinates are from PDB entry 4V88.

Results

Protein binding to *S. cerevisiae* ES7

S. cerevisiae cell lysates were screened for proteins with affinity for ES7 using pull-down assays. Mass spectrometry (MS) was used to identify ES7-associated proteins extracted from the lysates. During exponential growth of *S. cerevisiae*, 36 proteins (Table S.6) were seen to interact with ES7. Our assay identifies primary proteins that interact directly with ES7 in addition to secondary proteins that bind to the primary proteins.

As an illustration of the process used here for identifying ES7-associated proteins, a tandem mass spectrum corresponding to a peptide from lysyl-tRNA synthetase (LysRS) is shown in Fig. S.1. We attached isolated ES7 to beads, incubated the beads with cell lysates, washed the beads to remove non-specific and weakly associated proteins, and then proteolytically digested the ES7-associated proteins. The peptide ELELNFSRPWK was identified with an XCorr of 3.0 and a mass accuracy of -0.69 ppm. XCorr values represent the correlation between tandem mass spectra recorded in our experiment and the corresponding theoretic spectra of peptides in the database. The higher the XCorr, the greater the confidence in peptide identification. Similarly, mass accuracies determine the extent to which theoretical masses match observed masses of peptides in our experiments. Mass accuracies of less than 3 ppm indicate high confidence in peptide identification.

Many of the proteins seen here to associate with ES7 have been previously shown to bind to the

ribosome. Of the 36 ES7-associated proteins here, 25 were identified by Link as components of intact translation complexes [17]. These proteins include aspartyl tRNA synthetase (AspRS), translation machinery-associated protein 10 (TMA10), ribosome biogenesis protein ERB1 and ATP-dependent RNA helicase MAK5. Of these, 12 of them were identified as mRNA-binding proteins (mRBPs) by Hentze [18]. Nine proteins that associate with ES7 in this work were previously found to associate both with intact ribosomes and with mRNA [17,18]. Those nine are (i) protein transport factor SEC1; (ii) MAK21, which is involved in maturation and export of pre-LSU particles; (iii) fimbrin, which is an actin-bundling protein involved in cytoskeleton organization and maintenance; (iv) HXK1, which catalyzes hexose phosphorylation; (v) NAD(+) salvage pathway component, nicotinamide; (vi) transcription elongation factor SPT6; (vii) AspRS; (viii) 40S ribosomal protein S30; and (ix) protein PBI2, inhibitor of vacuolar protein B.

Seven aminoacyl tRNA synthetases (aaRSs) were identified here in association with ES7. AspRS and tyrosyl tRNA synthetase (TyrRS) were found in each of the replicate experiments. Cumulatively Ala-, Arg-, Asn-, Asp-, Leu-, Lys- and TyrRS were observed in at least one experiment. Our observations are consistent with Link *et al.*, [17] who observed Ala-, Asn-, Asp-, Leu- and LysRS bound to intact ribosomes. AspRS, LeuRS, and LysRS associate more tightly with the intact ribosome than AlaRS and AsnRS. The binding of AspRS, TyrRS and LysRS to ES7 is confirmed here by *in vitro* binding assays (below).

A total of six proteins known to localize in the nucleolus [19] are observed here to associate with ES7. Nucleolar proteins that associate with ES7

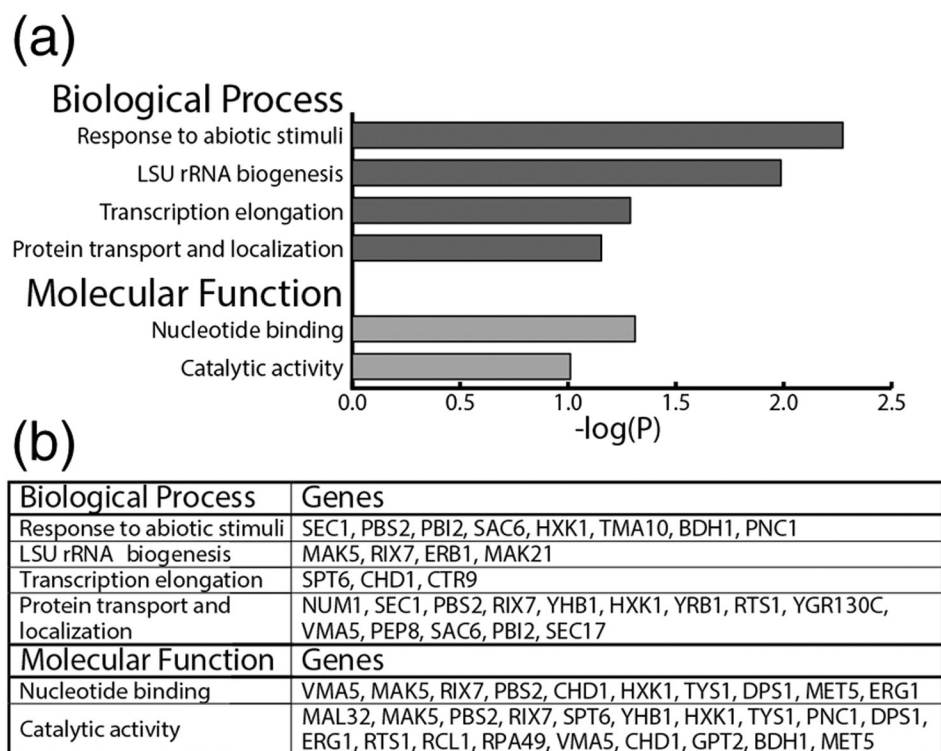


Fig. 3. Clustering of *S. cerevisiae* ES7-associated proteins identified in this work, based on biological process and molecular function. (a) Clusters were organized based on their P -values. A greater $-\log(P)$ corresponds to higher statistical significance. (b) List of genes included in each cluster.

include (i) MAK5, (ii) MAK21, (iii) ERB1, (iv) ribosome biogenesis ATPase RIX7, (v) DNA-directed RNA polymerase I subunit RPA49 and (vi) RNA 3'-terminal phosphate cyclase-like protein RCL1.

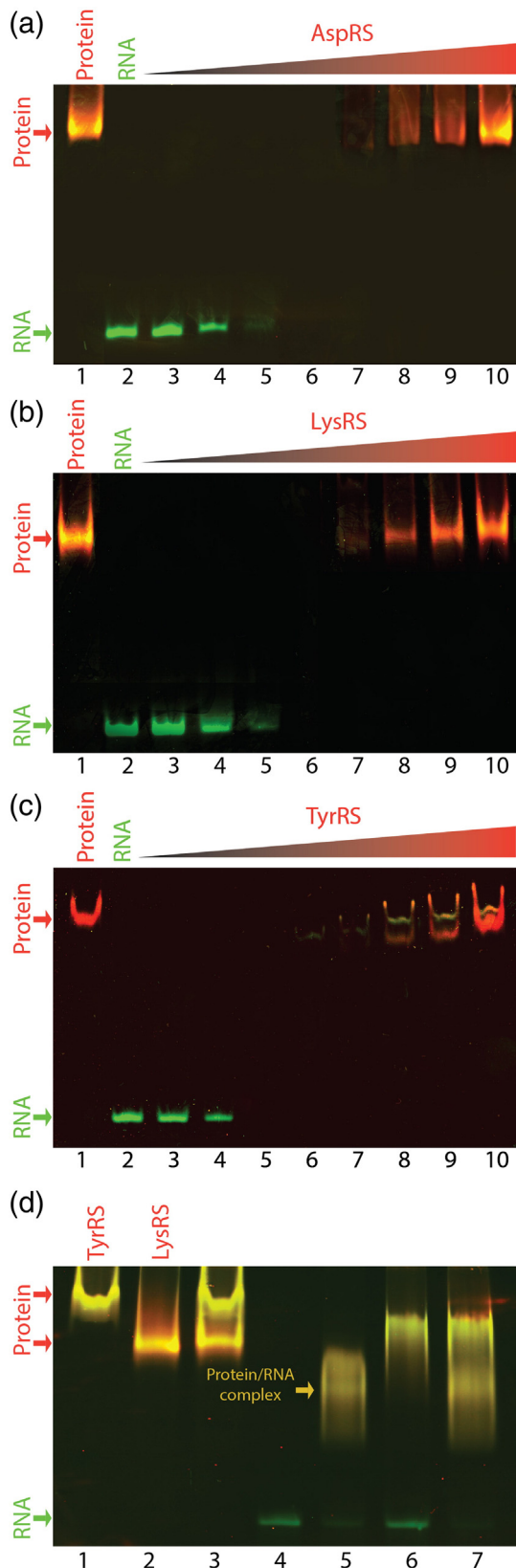
Clustering of ES7-associated proteins by biological process was performed using the Database for Annotation, Visualization and Integrated Discovery (DAVID) [20,21]. Four clusters are highly enriched (Fig. 3), including (i) response to abiotic stimulus such as temperature, (ii) ribosomal LSU biogenesis, (iii) protein transport and localization, and (iv) transcription elongation. For this analysis, if multiple clusters contained identical proteins, only the cluster with the lowest P -value was retained. The two most intense clusters correspond to response to abiotic stimulus ($P = 5.3 \times 10^{-3}$) and ribosomal LSU biogenesis ($P = 1.03 \times 10^{-2}$). Clusters with P -values lower than 0.05 are considered to be highly enriched and thus specifically associated with the corresponding biological process. With DAVID we were unable to cluster all 36 ES7-associated proteins because the functional annotation for the *S. cerevisiae* proteome is not fully finalized in the database. Of the 36 ES7-associated proteins, 12 were not clustered. Six mitochondrial proteins observed were assumed to be artifacts and were excluded from the analysis.

For comparison, we clustered Hentze's mRBPs by the same methods we used here for ES7-associated proteins, and we observed some of the same clusters.

Clusters common to mRBPs and ES7-associated proteins include (i) response to abiotic stimulus and (ii) protein transport and localization. ES7-associated proteins were also clustered based on molecular function with DAVID (Fig. 3). The results demonstrate that ES7-associated proteins are important in (i) nucleotide binding and (ii) catalytic activity. Both of these clusters are also seen in mRBPs.

S. cerevisiae* ES7 forming complexes with tRNA synthetases *in vitro

To assess the validity of the results of the pull-down experiments, and to determine if some of the associations are direct or are mediated by other proteins, we selected three ES7-associated proteins and assayed their affinities for ES7 *in vitro*. The affinities of Asp-, Lys- and TyrRS for ES7 were assayed by electrophoretic mobility shift assay (EMSA). The results (Fig. 4) demonstrate that AspRS, LysRS, and TyrRS bind tightly to ES7 and suggest that the interactions we detect are direct and not mediated by other proteins. One μM of rRNA and 1 μM of protein produce a single shifted rRNA band. It is probable that aaRS proteins bind to ES7 rRNA with 1:1 stoichiometry. Control experiments show that the affinities of aaRSs for ES7 rRNA are 3 to 10 times greater than for a different fragment of rRNA (Fig. S.2).



For these 1:1 complexes, the gels were quantitated and the dissociation constants, K_d 's, were estimated to be approximately 100 nM for LysRS and 1 μ M for AspRS and TyrRS. The affinities of these aaRS proteins for ES7 are roughly equivalent to the affinities observed elsewhere for ribosomal proteins for cognate rRNA [22,23]. K_d 's in the low micromolar to nanomolar ranges have been observed for ribosomal proteins uL1, uL2, uL3 and uL6 with rRNA.

Multi-protein EMSA experiments do not provide evidence of simultaneous binding of multiple aaRSs to ES7 (Figs. 4d and S.3). LysRS and TyrRS were selected for this assay based on the differential migration of the free proteins in native-PAGE. A fixed amount of ES7 RNA was incubated with TyrRS, LysRS and a combination of TyrRS and LysRS. The mobilities of LysRS and TyrRS alone differ from the mobility of the ES7-LysRS and ES7-TyrRS complexes. Incubation of ES7 simultaneously with TyrRS and LysRS showed at least two distinct bands that correspond to ES7-LysRS and ES7-TyrRS complexes. Bands suggesting the formation of additional ES-aaRS complexes could not be observed. The data do not support the formation of the ES7-LysRS-TyrRS complex.

Secondary structure of ES7

Selective 2'-hydroxyl acylation analyzed by primer extension (SHAPE) footprinting [24,25], computational folding [26] and phylogenetic data were used to determine the secondary structure of isolated *S. cerevisiae* ES7, which is seen to be the same as the ES7 secondary structure in the Yusupov three-dimensional structure [27] and the secondary structure of purified ribosomes determined by Dinman [28]. SHAPE monitors relative reactivity of 2'-oxygens to an electrophile, indicating the extent of local flexibility. Nucleotides in unpaired loops and bulges and in non-canonical base pairs show elevated SHAPE reactivity, while canonical helical regions

Fig. 4. EMSA of *S. cerevisiae* ES7 RNA with aaRSs. Binding of ES7 to (a) AspRS, (b) LysRS, (c) TyrRS, and (d) LysRS and TyrRS is shown. RNA, protein and RNA-protein complexes were visualized by two-color EMSA in native gels. Binding reactions for panels (a-c) were performed with 1 μ M RNA and various concentrations of protein. Lane 1 contains 10 μ M of protein and no RNA. Lane 2 consists of 1 μ M RNA only. Lanes 3-10 contain 1 μ M RNA and increasing protein concentration: lane 3 - 0.25 μ M protein, lane 4 - 0.50 μ M, lane 5 - 1 μ M, lane 6 - 2 μ M, lane 7 - 4 μ M, lane 8 - 6 μ M, lane 9 - 8 μ M, and lane 10 - 10 μ M. Binding reactions for panel (d) were performed with 4 μ M RNA and 10 μ M of each protein. Lane 1 contains 10 μ M of TyrRS, Lane 2 contains 10 μ M of LysRS, and Lane 3 contains 10 μ M of TyrRS and 10 μ M of LysRS. Lanes 4-7 contain 4 μ M RNA and various aaRSs: lane 4 - no protein, lane 5 - 10 μ M TyrRS, lane 6 - 10 μ M LysRS, and lane 7 - 10 μ M TyrRS and 10 μ M LysRS.

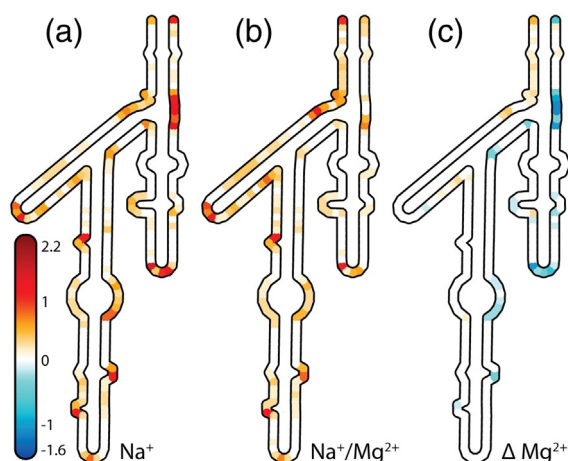


Fig. 5. SHAPE reactivities in Na^+ only and in $\text{Na}^+/\text{Mg}^{2+}$ reveal Mg^{2+} -dependent structural changes of *S. cerevisiae* ES7 rRNA. SHAPE reactivities are mapped onto ES7 rRNA secondary structure. Shape reactivities were determined in the presence of (a) Na^+ or (b) Na^+ and Mg^{2+} . Orange or red nucleotides show moderate to high SHAPE reactivity. Ivory or white nucleotides show low or no SHAPE reactivity. (c) Mg^{2+} induces changes in SHAPE reactivity. Nucleotides in red show increased reactivity in the presence of Mg^{2+} . Nucleotides in blue show decreased reactivity. These figures were generated with RiboVision [46]. All samples contained 200 mM NaOAc and 50 mM Na-HEPES at pH 8.

show depressed SHAPE reactivity. A direct comparison of the SHAPE reactivity of isolated ES7 to that of Dinman's ES7 secondary structure demonstrates that the secondary structure of isolated ES7 *in vitro* is the same as in intact ribosomes.

SHAPE reactivities were determined for all nucleotides of isolated *S. cerevisiae* ES7 (Fig. 5a). Nucleotides were clustered into three groups based on their SHAPE reactivity, after background subtraction and normalization. Positions of low SHAPE reactivity (<0.4) are located in helical regions in the secondary structure, whereas moderate and highly reactive SHAPE positions (>0.4) are concentrated in bulges, loops and RNA mismatches. The observed SHAPE data is fully consistent with the secondary model shown.

Tertiary structure

Changes in SHAPE reactivity suggest that Mg^{2+} induces formation of tertiary interactions in isolated ES7. Previously, the Mg^{2+} dependence of SHAPE reactivity was determined for a variety of RNAs including tRNA [29], RNase P [30], Domain III [31] and the intact LSU rRNA of *Thermus thermophilus* (Timothy K. Lenz, Nicholas Hud and Loren Williams, unpublished observations). The data were interpreted to indicate the formation of tertiary interactions upon addition of Mg^{2+} . We have used this comparative method to demonstrate specific inter-domain, intra-

domain and subunit folding of LSU rRNA caused by addition of Mg^{2+} [31,32].

SHAPE data obtained on ES7 in the presence of Na^+ alone (Fig. 5a) was subtracted from that obtained in the presence of Na^+ and Mg^{2+} (Fig. 5b). The heat map obtained by this method (Fig. 5c) identifies nucleotides that increase or decrease in reactivity upon addition of Mg^{2+} . It can be seen that canonical helical regions are invariant to the addition of Mg^{2+} , consistent with the expectation that secondary structure is maintained upon formation of tertiary structure. Changes in reactivity are focused on loops and non-helical regions, which are expected to be involved in tertiary interactions. The results suggest that isolated ES7 of *S. cerevisiae* forms tertiary interactions upon addition of Mg^{2+} .

Thermal folding/unfolding of *S. cerevisiae* ES7

Isolated ES7 is well behaved in solution. The number of transitions in the unfolding process provides information on the architecture of ES7. Thermal melts show that the folded structure is stable at room temperature and that folding and unfolding are reversible. Thermodynamic parameters were obtained from the melting curves by nonlinear fitting to a multi-state model with independent transitions (Fig. S.4) [33]. An estimate of the number of melting transitions and the thermodynamic parameters associated with these transitions is obtained from the melting profile, which is the derivative of the fraction unfolded (d/dT) as a function of temperature (Fig. 6). The best fit to the melting profile of ES7 was obtained with a four-transition model (Fig. 6). A three-transition unfolding model gives significantly worse statistics of fit. However, unfolding models with additional transitions cannot be excluded by the methods used here and, in fact, are probable for such a large RNA.

Melting profiles were fit and deconvoluted to obtain estimates of thermodynamic parameters for each of the four transitions. The melting temperatures ($T_{m,n}$) of the transitions are $T_{m,1} = 51^\circ\text{C}$, $T_{m,2} = 64^\circ\text{C}$, $T_{m,3} = 75^\circ\text{C}$, and $T_{m,4} = 83^\circ\text{C}$ in 180 mM NaCl. The highest temperature transition has a relatively small hyperchromicity but was retained in the model because it is reproducible and is observed in the thermal melting of isolated ES7 rRNA from a closely related fungi (unpublished observations). In this method, uncertainty arises because enthalpies can correlate with hyperchromicities [33]. The T_m 's are constant with varying RNA concentrations (unpublished observations) indicating that the transitions are unimolecular. Since ES7 rRNA is large and is subject to degradation, Mg^{2+} was excluded from melting buffers to prevent in-line cleavage [34]. Additional information on thermodynamic models and parameter estimation is provided in Supplementary Materials.

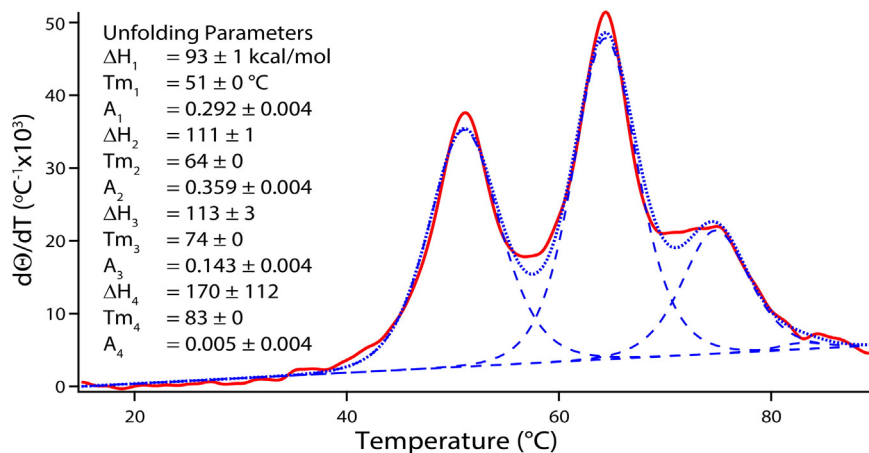


Fig. 6. Melting profile of *S. cerevisiae* ES7 rRNA. The derivative of fraction unfolded at 260 nm with respect to temperature was computed. The derivative was fit to a non-sequential, independent transition model with Igor v.6.37. The enthalpy (ΔH_n), melting temperature ($T_{m,n}$) and the relative hyperchromicity (A_n) were estimated for each transition, n . The observed derivative is shown in red, the fit is shown in dotted blue, and the deconvolution of the fit is shown in dashed blue.

Discussion

Mammals have the largest known rRNAs. Metazoans have larger rRNAs than protists, which have larger rRNAs than prokaryotes. We suggest that the breadth of ribosomal function is related to the size of the rRNA [4] and that eukaryotic ribosomes facilitate functions that are auxiliary to translation. One of the foci of rRNA expansion is ES7. By determining which proteins associate with ES7 we can deduce at least some of its contributions to function.

At least 36 proteins in cell lysates bind to isolated ES7 rRNA of *S. cerevisiae* directly or through intermediates. Of these ES7-associated proteins, 25 were previously identified by Link in association with intact ribosomes [17]. It appears that we have identified the subset of Link's proteins that bind to ES7 rRNA as opposed to other regions of the ribosome. Of the ES7-associated proteins observed here, 12 were also identified as mRBPs by Hentze [18]. Some proteins identified here may bind at multiple sites on the ribosome. Six of the ES7-associated proteins reside in the nucleolus, consistent with roles of ES7 in ribosome biogenesis [35].

ES7-associated proteins were clustered with DAVID [21,36] into four groups based on biological process, (i) response to abiotic stimulus such as temperature, (ii) LSU ribosomal biogenesis, (iii) protein transport and localization, and (iv) transcription elongation (Fig. 3). Clustering based on molecular function shows that ES7-associated proteins are important in nucleotide binding and catalytic activity.

aaRSs

aaRSs couple amino acids with their cognate tRNAs, establishing the relationship of nucleotide triplets with

amino acids (i.e., the genetic code). Cumulatively, seven synthetases, Ala-, Arg-, Asp-, Asn-, Leu-, Lys- and TyrRS were observed in at least one experiment. ES7 may be a focus of aaRS association on the ribosome. Previously, 16 aaRSs were observed to associate with intact ribosomes in *S. cerevisiae* [17]. ES7 may be an ancestor or proxy of large multi-aaRS complexes in other systems, maintaining close association of synthetases with each other and with the translational machinery. In *S. cerevisiae*, only two aaRSs are found in the multi-synthetase complex [37]. These two aaRSs are not observed here to associate with ES7. Half of the ES7-associated aaRSs in *S. cerevisiae* correspond with those observed previously in the human multi-aaRS complex [38]. Yeast two-hybrid studies in archaea suggest that EF-1 α associates with LeuRS and contributes to the overall translation efficiency by promoting aminoacylation [39]. Our work complements these findings. ES7 could act as a hub for tRNA aminoacylation and for improving translation efficiency.

Affinity and specificity of AspRS, TyrRS and LysRS for ES7 were confirmed by *in vitro* binding assays. AspRS and TyrRS were observed in each of the replica experiments and appear to be the most robust ES7 binders. The affinities and specificities of AspRS, LysRS, and TyrRS for ES7 were assayed by EMSA. The data suggest that these aaRS proteins bind to ES7 rRNA with 1:1 stoichiometry. Their affinities for ES7 are greater than for a different rRNA fragment (Fig. S.2). The results also suggest that these three aaRSs bind directly to ES7, supporting the hypothesis that ES7 in *S. cerevisiae* might promote close association of aaRSs with each other and with the ribosome. Based on the direct association of ES7 to Asp-, Lys- and TyrRS it seems likely that additional aaRSs might bind

to ES7 *in vivo* and may form stable RNA-protein complexes. Multi-protein EMSA does not provide evidence for simultaneous association of ES7 with multiple aaRSs.

Observations of RNA-protein association in pull-down experiments must account to control for non-specific RNA-protein binding. A complex observed experimentally might not be relevant *in vivo* because of competition from other factors. Several measures were taken to control non-specific RNA-protein binding. For a subset of the ES7-associated proteins we have directly confirmed high affinities *in vitro* (Figs. 4, S.2, and S.3). ES7 has 26,000 Å² of accessible surface area when stripped of ribosomal proteins and 20,000 Å² of accessible surface area in the assembled ribosome. Therefore ES7 provides ample surface area for association with non-ribosomal proteins. Considering that rRNA accounts for over 80% of cellular RNA [40], competition from other RNAs seems unlikely, and the proteins detected here must be considered highly probable ES7 binding partners *in vivo*. However, binding of proteins could be transient and might depend upon the stage cell cycle and on external cell environment. We expect that the majority of the proteins identified in this study are representative of the proteins that bind to ES7 *in vivo* during log phase, although we cannot exclude additional binding partners.

Ribosomal proteins

Although some nucleolar proteins were identified, it seems likely that nucleoli and intact nuclei were depleted prior to the assay. None of the ES7-associated proteins found here are ribosomal proteins. ES7 rRNA does contact multiple ribosomal proteins in the assembled ribosome (Fig. 2). rProtein uL4 makes the most extensive contacts with ES7, yet it is not observed in our assay. It is possible that uL4 in the cytoplasm is tied up in association with ribosomes, and that the amount of free uL4 not associated with assembled LSU, is sufficiently small that it cannot be detected in our assay.

ES7 folding

Our footprinting and folding/unfolding experiments along with computational studies indicate that isolated ES7 folds to a native-like secondary structure, consistent with the secondary structure inferred for intact *S. cerevisiae* ribosomes [27,28]. In the presence of Mg²⁺, isolated ES7 forms tertiary interactions. The thermal melting shows that folded ES7 is highly stable and that the multistate folding/unfolding process is reversible. Altogether, the results provide experimental confirmation of the secondary structure of *S. cerevisiae* ES7 and suggest that our experiments employed a native-like structure of ES7 rRNA.

Conclusions

We hypothesize that expansion segments could be sites of functional interactions with other macromolecules given their proximity to the ribosome surface. ES7 is the largest expansion segment and the most variable region of rRNA over phylogeny. We performed *in vitro* characterization of *S. cerevisiae* ES7 by measuring its stability and its interactions with cellular proteins. The results here support our hypothesis. Here, we demonstrate that Asp-, Lys- and TyrRS bind directly to *S. cerevisiae* ES7. aaRSs charge amino acids with their cognate tRNAs catalyzing the first reaction needed for protein synthesis [41]. Therefore, expansion segments likely play a variety of important roles in protein synthesis.

Materials and Methods

S. cerevisiae ES7 DNA and RNA

The DNA encoding *S. cerevisiae* ES7 was amplified from yeast genomic DNA. The T7 promoter and restriction sites for EcoRI (5' end) and HindIII (3' end) were added via PCR. The DNA was inserted into a previously restricted, dephosphorylated pUC19 plasmid. Ligated plasmid was transformed into DH5α competent cells and colonies were selected based on X-gal Blue-White screening (Thermo Scientific). Primer sequences are shown in Table S.1.

The Weeks cassette [42] was incorporated onto the 3' end of ES7 to allow SHAPE mapping without losing information from ES7 termini using the Q5® Site-directed Mutagenesis Kit (New England BioLabs). Primer information is described in Table S.2. Primer synthesis and DNA sequencing were performed by Eurofins-MWG Operon.

In vitro RNA synthesis

S. cerevisiae ES7 RNAs were transcribed (HiScribe™ T7 High Yield RNA Synthesis Kit, New England BioLabs) with the following modifications to the manufacturer's protocol. pUC19 containing the *S. cerevisiae* ES7 gene was linearized at the 3' end with HindIII. In each 20 μL transcription reaction, 500 ng of DNA template were used. The DNA was transcribed overnight at 37 °C, followed by incubation with TURBO DNase (Ambion) at 37 °C for 15 min. A 1:10 dilution of a 5 M ammonium acetate solution (pH 5.6) and 2.5 vol of 100% ethanol were added to the reaction mixture, which was then incubated at -20 °C for 1 h and centrifuged at 15,600g for 10 min at 4 °C. Pellets were washed three times with 80% ethanol before drying via Speedvac. RNA was resuspended in nuclease-free water and then purified from unincorporated nucleotides with an illustra NAP 5 column (GE

Healthcare). RNA yields were quantified by UV absorbance. RNA purity and integrity were verified by 6% acrylamide (29:1 acry:bisacryl) and 8 M urea gel with TBE buffer.

SHAPE reactions

SHAPE methods were adapted from published protocols [32,42]. *In vitro*-transcribed RNA in nuclease-free water was added to folding buffer [final concentrations: 200 mM NaOAc, 50 mM Na-HEPES (pH 8.0), and 1 mM 1,2-trans- cyclohexane-N,N,N',N'-diaminetetraacetic acid or 5 mM of MgCl₂] to obtain 400 nM RNA in 80 μ L. RNAs were annealed by cooling from 75 °C to 25 °C at 1 °C/min. Data were collected in 200 mM Na⁺ and no magnesium to analyze secondary structure [43–45]. RNA tertiary interactions were characterized in the presence of Mg²⁺ ions.

Benzoyl cyanide reaction

Chemical modification of ES7 RNA was performed with a 10 \times dilution of a 1000mM benzoyl cyanide (Sigma) stock prepared in dimethyl sulfoxide (DMSO) into 36 μ L of annealed RNA. Control reactions contained DMSO only. Reactions were carried out for ~1–2 min at room temperature [30].

Benzoyl-cyanide-modified RNA was purified from reaction mixtures by precipitation in ammonium acetate [1:10 dilution, 3 M (pH 5.2)] and ethanol (2.5 vol.) at 20 °C for ~15 min. Reaction mixtures were centrifuged at 15,600g at 4 °C for 10 min, and the pellet was washed once with 80% ethanol before drying via Speedvac. Pellets were resuspended in 22 μ L 1x TE buffer [10 mM Tris-Cl and 1 mM EDTA (pH 8.0)]. Recovery after purification was >40%.

Reverse transcription (RT) of benzoyl-cyanide-modified *S. cerevisiae* ES7 RNA

A single [6-FAM]-labeled primer (Table S.3) provided complete SHAPE reads on ES7 of *S. cerevisiae* [29]. Modified RNA (20 μ L) was added to 40 pmol primer in reverse transcription (RT) buffer to yield 1X First-Strand Buffer (Invitrogen), 2 mM DTT, and 625 μ M of each deoxynucleotidetriphosphate (dNTP) in 50 μ L. Primer annealing was performed stepwise: 95 °C for 30 secs, 65 °C for 3 min, 60 °C for 3 min, and 4 °C for 10 min. SuperScript III Reverse Transcriptase (Invitrogen) was used in RT reactions. RT mixtures were pre-incubated at 52 °C for 2 min before the addition of 1 μ L (200 U) of RT enzyme, and reaction was allowed to proceed for 2 h at 52 °C. RT enzyme was inactivated at 70 °C for 15 min. RT reactions were also performed on unmodified RNAs (DMSO only) at the conditions used for modified RNA samples.

RNA was sequenced by RT/chain termination using dideoxynucleotide (ddNTPs) at a ratio of 1:1 ddNTP to dNTP. For sequencing reactions, 10 pmol of ES7 RNA in TE buffer and 40 pmol of primer were used. A reaction without ddNTPs identified natural polymerase fall-off peaks.

Capillary electrophoresis of RT reaction products. Analysis of RT reaction productions was performed as described previously. [32].

SHAPE data processing. SHAPE data were processed as described [31]. SHAPE data were mapped onto secondary structures with the program RiboVision [46].

Folding/Unfolding

Melting curves for ES7 RNA were determined by measuring absorbance at 260 nm as a function of temperature with a thermostated Varian Cary-1E UV spectrophotometer. RNA was concentrated by Speedvac to at least 1 μ g/ μ L and was added to melting buffer [180 mM NaCl, 20 mM Tris-HEPES (pH 8.0)] to reach an initial absorbance of 0.30–0.33 at 260 nm. Samples were heated from 15 °C to 95 °C at 3 °C/min in the spectrophotometer to unfold the RNA. Melting transitions were obtained by repeated heating and cooling at 0.5 °C/min. Due to the RNA size, the temperature ramp was less than 1 °C/min, which is commonly used for melting short duplexes [47]. Superimposition of heating and cooling curves was used to confirm equilibrium during melting. Thermodynamic model information and the information on fitting and parameter estimation are described in the Supplementary Materials.

Pull-down assays and LC-MS/MS analysis

The DNA anchor was the same sequence as the SHAPE primer, modified with a biotin label on the 5' end (Table S.3). ES7 RNA (1.3 μ M) was annealed to 2 μ M of the DNA anchor in the buffer used to melt the RNA and annealed as described for SHAPE experiments. SoftLink™ Soft Release Avidin Resin (Promega) was washed three times with lysis buffer [0.1% (wt./vol.) sodium deoxycholate, 100 mM NaCl, 1 mM EDTA, 50 mM Tris-Cl (pH 8.0), and 1x protease inhibitor cocktail containing 1 mM AEBSF and 1.54 mM Aprotinin] also containing 10 U of RNase inhibitor, 5 mg/mL of heparin (Fisher Scientific) and 0.5 mg/mL of yeast tRNA (Roche) at 4 °C. Then, the RNA-biotin assembly was shaken gently at room temperature with 10 μ L of equilibrated Avidin resin to attach ES7 to the resin.

Pull-down assays were performed with *S. cerevisiae* cell lysates. One feature of these experiments that distinguishes them from conventional pull-down assays is the high abundance of the competing rRNA

within the lysate. It seems likely that intrinsic competition from endogenous rRNA might attenuate non-specific binding.

A starter culture of *S. cerevisiae* was grown in yeast extract-peptone-dextrose (YPD) media overnight at 30 °C and used to inoculate a 50 mL culture. Cells were harvested when they reached an optical density at 600 nm (OD₆₀₀) of ~1.0 by pelleting at 770g and 4 °C for 15 min. Pellets were stored at -80 °C until use. Cells were resuspended in lysis buffer and 0.5 mm Zirconia/Silica beads (BioSpec) were added. Cell lysis was performed on a Mini BeadBeater 16 (BioSpec) with three 30- 30 sec cycles and was interleaved by 2 min of incubation on ice. Lysates were separated from beads by centrifugation at 1000g for 3 min, vortexed and centrifuged at 15,000g for 10 min. The supernatant was collected and used for pull-down experiments.

To assay non-specific protein binding to Avidin or the biotinylated DNA anchor, we performed three parallel experiments, that is, three samples were incubated with the cell lysate: (1) Avidin-biotin primer-RNA, (2) Avidin only, and (3) Avidin-biotin primer complex. One hundred twenty µL of cell lysate were added to each reaction and incubated for one hour at room temperature with end-over-end rotation. Following incubation, samples were transferred to 30-µm polyethylene spin columns and washed three times with 200 µL of lysis buffer. Digestion buffer containing 50 mM HEPES (pH 7.5), 0.1 M urea and 5% acetonitrile was added to the samples and digestion was carried out overnight at 31 °C with Lys-C at a ~1:200 Lys-C:protein ratio. Flow-through digests were collected. Avidin beads on spin columns were washed twice with a solution containing 75% acetonitrile and 0.5% acetic acid, and all flow-through was collected and combined for each sample. Acetonitrile was removed by evaporation and the peptides were purified with the stage tip method [48] and dried again. Purified samples were dissolved in 5% acetonitrile and 1% formic acid for liquid chromatography tandem mass spectrometry (LC-MS/MS). Further details on LC-MS/MS runs and data analysis are found in the Supplementary Materials.

EMSA

Cloning of tRNA synthetases

The cDNA for *S. cerevisiae* aspartyl-tRNA synthetase (AspRS), lysyl-tRNA synthetase (LysRS) and tyrosyl-tRNA synthetase (TyrRS) was obtained from DNASU plasmid repository [49]. Synthetase DNA was amplified by PCR to add NdeI and XhoI restriction sites at the 5' and 3' ends of the corresponding genes and cloned into pET21b (Novagen) with a C-terminal 6x histidine tag. Primer sequences are described in Table S.4. *E. coli* BL21 (DE3) transformants were selected based on ampicillin resistance (50 µg/mL) and screened for insert by colony PCR.

tRNA-synthetase expression and purification

Three mL starter cultures of *E. coli* BL21 (DE3) transformed cells were incubated overnight at 37 °C with 50 µg/mL ampicillin. These cultures were used to inoculate (1% v/v) 100 mL cultures in a shaking incubator at 37 °C until OD₆₀₀ reached 0.5–0.7. Expression was induced by the addition of 0.5 mM final concentration of isopropyl β-D-1-thiogalactopyranoside (IPTG) and cultures were incubated for 4 h at 37 °C. Cells were harvested by spinning at 4 °C and 3900g for 15 min. Pellets were stored at -80 °C until use.

Protein purification was carried out by standard immobilized metal affinity chromatography (IMAC). Cell pellets were resuspended in 5 mL of 50 mM sodium phosphate, 300 mM NaCl, and 20 mM imidazole at pH 8.0. Cell lysis was performed in ice water by sonication with QSonica Q125 at 50% amplitude for 30 sec, nine times, with 30 sec intervals, followed by centrifugation in a Sorvall RC 5Bplus centrifuge at 23,426g for 30 min at 4 °C. Clarified cell lysate was bound to 1 mL of Ni-NTA resin with gentle rocking at 4 °C for 45 min, and then purified with column chromatography. The resin was washed two times with five column volumes (CVs) of 50 mM sodium phosphate (pH 8.0), 300 mM NaCl, and 50 mM imidazole. Protein was eluted with 0.5 CVs of 50 mM sodium phosphate (pH 8.0), 300 mM NaCl, and 250 mM imidazole. Protein concentration was measured by BCA [50]. Active fractions were concentrated and stored in 50% (v/v) glycerol. Protein purity and integrity were analyzed by sodium dodecyl sulfate polyacrylamide gel electrophoresis (SDS-PAGE).

ES7 rRNA/aaRSs interactions

RNA-protein interactions were characterized by EMSA as described previously [32] with the following modifications. A 10µM solution of ES7 RNA was prepared in 20 mM Tris-HEPES (pH 8.0) and annealed by cooling from 90 °C to 25 °C at 2 °C/min. aaRSs were introduced at varying concentrations (0.25 µM–10 µM final) and incubated with 1 µM of ES7 RNA (final concentration) for 20 min at room temperature. Multi-protein EMSA was performed with fixed RNA (4 µM) and fixed protein concentration (10 µM LysRS and 10 µM TyrRS) in 20 mM Tris-HEPES (pH 8.0). RNA-protein incubation was also performed for 20 min at room temperature. RNA-protein interactions were analyzed on 5% native-PAGE with 3% glycerol. Gels were visualized using a two-color fluorescent dye protocol in a Typhoon FLA 9500 (GE Healthcare) [51]. In a two-color fluorescent EMSA, uncomplexed nucleic acid is green, free protein is red and the nucleic acid protein complexes are yellow, although slight

leaking between channels of the Typhoon imager was observed. Control reactions used a fragment of Domain III rRNA from *T. thermophilus*.

Acknowledgements

S. cerevisiae genomic DNA was kindly provided by Dr. Kirill S. Lobachev. The authors thank Dr. Timothy K. Lenz for helpful discussions on SHAPE experiments and analysis, Eric B. O'Neill for helpful discussion on RNA transcription and purification, and Dr. Anton S. Petrov and Dr. Chad Bernier for discussions of ribosomal structure and variability. R.W. acknowledges Georgia Tech and the Blanchard Assistant Professorship. L.M.G.R. acknowledges funding through National Science Foundation Graduate Research Fellowship (Grant No. DGE-1148903) and the Alfred P. Sloan and GaTech UCEM Minority Doctoral Fellowship.

Author contributions

L.M.G.R., J.M.S., J.C.B., R.W., R.M.W., and L.D.W. conceived and designed the experiments; L.M.G.R. and J.M.S. performed the experiments; L.M.G.R., J.M.S., and N.A.K. analyzed data; L.M.G.R., J.M.S., N.A.K., and L.D.W. prepared the figures; and L.M.G.R., J.M.S., R.W., R.M.W., and L.D.W. wrote the paper.

The authors declare that they have no conflict of interest.

Appendix A. Supplementary Data

Supplementary data to this article can be found online at <http://dx.doi.org/10.1016/j.jmb.2016.08.008>.

Received 24 March 2016;

Received in revised form 4 August 2016;

Accepted 5 August 2016

Available online xxxx

Keywords:

aminoacyl tRNA synthetases;
rRNA expansion segments;
rRNA-protein interaction;
SHAPE;
thermal unfolding

Abbreviations used:

rRNA, ribosomal RNA; ES, expansion segment; LSU, large ribosomal subunit; ES7, expansion segment 7; aaRS, aminoacyl tRNA synthetase; AspRS, aspartyl tRNA synthetase; LysRS, lysyl tRNA synthetase; TyrRS, tyrosyl tRNA synthetase; mRBP, mRNA-binding protein; EMSA, electrophoretic mobility shift assay; SHAPE, selective 2'-hydroxyl acylation analyzed by primer extension; RT, reverse transcription.

References

- [1] C.J. Shoemaker, R. Green, Translation drives mRNA quality control, *Nat. Struct. Mol. Biol.* 19 (2012) 594–601.
- [2] M.Y. Sherman, S.-B. Qian, Less is more: improving proteostasis by translation slow down, *Trends Biochem. Sci.* 38 (2013) 585–591.
- [3] S. Pechmann, F. Willmund, J. Frydman, The ribosome as a hub for protein quality control, *Mol. Cell.* 49 (2013) 411–421.
- [4] A.S. Petrov, C.R. Bernier, C. Hsiao, A.M. Norris, N.A. Kovacs, C.C. Waterbury, et al., Evolution of the ribosome at atomic resolution, *Proc. Natl. Acad. Sci. U. S. A.* 111 (2014) 10,251–10,256.
- [5] V.C. Ware, B.W. Tague, C.G. Clark, R.L. Gourse, R.C. Brand, S.A. Gerbi, Sequence analysis of 28S ribosomal DNA from the amphibian *Xenopus laevis*, *Nucleic Acids Res.* 11 (1983) 7795–7817.
- [6] C.G. Clark, B.W. Tague, V.C. Ware, S.A. Gerbi, *Xenopus laevis* 28S ribosomal RNA: a secondary structure model and its evolutionary and functional implications, *Nucleic Acids Res.* 12 (1984) 6197–6220.
- [7] N. Hassouna, B. Michot, J.P. Bachelierie, The complete nucleotide sequence of mouse 28S rRNA gene. Implications for the process of size increase of the large subunit rRNA in higher eukaryotes, *Nucleic Acids Res.* 12 (1984) 3563–3583.
- [8] S.A. Gerbi, Expansion segments: regions of variable size that interrupt the universal core secondary structure of ribosomal RNA, in: RA Zimmermann, AE Dahlberg (Eds.), *Ribosomal RNA—Structure, Evolution, Processing, and Function in Protein Synthesis*, CRC Press, Boca Raton, FL 1996, pp. 71–87.
- [9] S. Melnikov, A. Ben-Shem, N. Garreau de Loubresse, L. Jenner, G. Yusupova, M. Yusupov, One core, two shells: bacterial and eukaryotic ribosomes, *Nat. Struct. Mol. Biol.* 19 (2012) 560–567.
- [10] A. Ben-Shem, L. Jenner, G. Yusupova, M. Yusupov, Crystal structure of the eukaryotic ribosome, *Science*, 330 (2010) 1203–1209.
- [11] H. Han, A. Schepartz, M. Pellegrini, P.B. Dervan, Mapping RNA regions in eukaryotic ribosomes that are accessible to methidiumpropyl-EDTA. Cntdot. Fe (II) and EDTA. Cntdot. Fe (II), *Biochemistry* 33 (1994) 9831–9844.
- [12] R. Sweeney, L. Chen, M.-C. Yao, An rRNA variable region has an evolutionarily conserved essential role despite sequence divergence, *Mol. Cell. Biol.* 14 (1994) 4203–4215.
- [13] R.E. Jeeninga, Y. Van Delft, M. de Graaff-Vincent, A. Dirks-Mulder, J. Venema, H.A. Raué, Variable regions v13 and v3 of *Saccharomyces cerevisiae* contain structural features essential for normal biogenesis and stability of 5.8 s and 25 s rRNA, *RNA* 3 (1997) 476–488.
- [14] M. Ramesh, J.L. Woolford, Eukaryote-specific rRNA expansion segments function in ribosome biogenesis, *RNA* 22 (2016) 1–10.
- [15] H. Gao, M.J. Ayub, M.J. Levin, J. Frank, The structure of the 80S ribosome from *Trypanosoma cruzi* reveals unique rRNA components, *Proc. Natl. Acad. Sci. U. S. A.* 102 (2005) 10,206–10,211.
- [16] Y. Hashem, A. des Georges, J. Fu, S.N. Buss, F. Jossinet, A. Jobe, et al., High-resolution cryo-electron microscopy structure of the *Trypanosoma brucei* ribosome, *Nature* 494 (2013) 385–389.
- [17] T.C. Fleischer, C.M. Weaver, K.J. McAfee, J.L. Jennings, A.J. Link, Systematic identification and functional screens of

- uncharacterized proteins associated with eukaryotic ribosomal complexes, *Genes Dev.* 20 (2006) 1294–1307.
- [18] B.M. Beckmann, R. Horos, B. Fischer, A. Castello, K. Eichelbaum, A.M. Alleaume, et al., The RNA-binding proteomes from yeast to man harbour conserved enigmrbps, *Nat. Commun.* 6 (2015) 10,127.
- [19] W.-K. Huh, J.V. Falvo, L.C. Gerke, A.S. Carroll, R.W. Howson, J.S. Weissman, et al., Global analysis of protein localization in budding yeast, *Nature*, 425 (2003) 686–691.
- [20] D.W. Huang, B.T. Sherman, R.A. Lempicki, Systematic and integrative analysis of large gene lists using David bioinformatics resources, *Nat. Protoc.* 4 (2009) 44–57.
- [21] D.W. Huang, B.T. Sherman, R.A. Lempicki, Bioinformatics enrichment tools: paths toward the comprehensive functional analysis of large gene lists, *Nucleic Acids Res.* 37 (2009) 1–13.
- [22] C. Köhrer, C. Mayer, O. Neumair, P. Gröbner, W. Piendl, Interaction of ribosomal L1 proteins from mesophilic and thermophilic archaea and bacteria with specific L1-binding sites on 23S rRNA and mRNA, *Eur. J. Biochem.* 256 (1998) 97–105.
- [23] T. Uchiumi, N. Sato, A. Wada, A. Hachimori, Interaction of the sarcin/ricin domain of 23 s ribosomal RNA with proteins L3 and L6, *J. Biol. Chem.* 274 (1999) 681–686.
- [24] K.A. Wilkinson, S.M. Vasa, K.E. Deigan, S.A. Mortimer, M.C. Giddings, K.M. Weeks, Influence of nucleotide identity on ribose 2'-hydroxyl reactivity in RNA, *RNA*, 15 (2009) 1314–1321.
- [25] K.M. Weeks, D.M. Mauger, Exploring RNA structural codes with SHAPE chemistry, *Acc. Chem. Res.* 44 (2011) 1280–1291.
- [26] M. Zuker, Mfold web server for nucleic acid folding and hybridization prediction, *Nucleic Acids Res.* 31 (2003) 3406–3415.
- [27] A. Ben-Shem, N.G. de Loubresse, S. Melnikov, L. Jenner, G. Yusupova, M. Yusupov, The structure of the eukaryotic ribosome at 3.0 Å resolution, *Science*, 334 (2011) 1524–1529.
- [28] J.A. Leshin, R. Heselpoth, A.T. Belew, J. Dinman, High throughput structural analysis of yeast ribosomes using hshape, *RNA Biol.* 8 (2011) 478–487.
- [29] E.J. Merino, K.A. Wilkinson, J.L. Coughlan, K.M. Weeks, RNA structure analysis at single nucleotide resolution by selective 2'-hydroxyl acylation and primer extension (SHAPE), *J. Am. Chem. Soc.* 127 (2005) 4223–4231.
- [30] S.A. Mortimer, K.M. Weeks, Time-resolved RNA SHAPE chemistry, *J. Am. Chem. Soc.* 130 (2008) 16,178–16,180.
- [31] S.S. Athavale, J.J. Gossett, C. Hsiao, J.C. Bowman, E. O'Neill, E. Hershkovitz, et al., Domain III of the *T. thermophilus* 23S rRNA folds independently to a near-native state, *RNA* 18 (2012) 752–758.
- [32] C. Hsiao, T.K. Lenz, J.K. Peters, P.Y. Fang, D.M. Schneider, E.J. Anderson, et al., Molecular paleontology: a biochemical model of the ancestral ribosome, *Nucleic Acids Res.* 41 (2013) 3373–3385.
- [33] D.E. Draper, Y.V. Bukhman, T.C. Gluick, Thermal methods for the analysis of RNA folding pathways, *Curr. Protoc. Nucleic Acid Chem* (2001) 11.3.1–11.3.13.
- [34] M. Forconi, D. Herschlag, Metal ion-based RNA cleavage as a structural probe, *Methods Enzymol.* 468 (2009) 91–106.
- [35] U. Ohmayer, Á. Gil-Hernández, M. Sauert, P. Martín-Marcos, M. Tamame, H. Tschochner, et al., Studies on the coordination of ribosomal protein assembly events involved in processing and stabilization of yeast early large ribosomal subunit precursors, *PLoS One* 10 (12) (2015), e0143768, <http://dx.doi.org/10.1371/journal.pone.0143768>.
- [36] D.J. Taylor, B. Devkota, A.D. Huang, M. Topf, E. Narayanan, A. Sali, et al., Comprehensive molecular structure of the eukaryotic ribosome, *Structure* 17 (2009) 1591–1604.
- [37] S. Havrylenko, M. Mirande, Aminoacyl-tRNA synthetase complexes in evolution, *Int. J. Mol. Sci.* 16 (2015) 6571–6594.
- [38] S.W. Lee, B.H. Cho, S.G. Park, S. Kim, Aminoacyl-tRNA synthetase complexes: beyond translation, *J. Cell Sci.* 117 (2004) 3725–3734.
- [39] C.D. Hausmann, M. Prætorius-Ibba, M. Ibba, An aminoacyl-tRNA synthetase: elongation factor complex for substrate channeling in archaeal translation, *Nucleic Acids Res.* 35 (2007) 6094–6102.
- [40] J.R. Warner, The economics of ribosome biosynthesis in yeast, *Trends Biochem. Sci.* 24 (1999) 437–440.
- [41] P.R. Schimmel, D. Soll, Aminoacyl-tRNA synthetases: general features and recognition of transfer RNAs, *Annu. Rev. Biochem.* 48 (1979) 601–648.
- [42] K.A. Wilkinson, E.J. Merino, K.M. Weeks, Selective 2'-hydroxyl acylation analyzed by primer extension (SHAPE): quantitative RNA structure analysis at single nucleotide resolution, *Nat. Protoc.* 1 (2006) 1610–1616.
- [43] P. Brion, E. Westhof, Hierarchy and dynamics of RNA folding, *Annu. Rev. Biophys. Biomol. Struct.* 26 (1997) 113–137.
- [44] G. Colmenarejo, I. Tinoco, Structure and thermodynamics of metal binding in the p5 helix of a group I intron ribozyme, *J. Mol. Biol.* 290 (1999) 119–135.
- [45] J.C. Bowman, T.K. Lenz, N.V. Hud, L.D. Williams, Cations in charge: magnesium ions in RNA folding and catalysis, *Curr. Opin. Struct. Biol.* 22 (2012) 262–272.
- [46] C. Bernier, A.S. Petrov, C. Waterbury, J. Jett, F. Li, L.E. Freil, et al., Ribovision: Visualization and analysis of ribosomes, *Faraday Discuss.* 169 (2014) 195–207.
- [47] J.D. Puglisi, I. Tinoco Jr., Absorbance melting curves of RNA, *Methods Enzymol.* 180 (1989) 304–325.
- [48] J. Rappsilber, M. Mann, Y. Ishihama, Protocol for micro-purification, enrichment, pre-fractionation and storage of peptides for proteomics using stagetips, *Nat. Protoc.* 2 (2007) 1896–1906.
- [49] C.Y. Seiler, J.G. Park, A. Sharma, P. Hunter, P. Surapaneni, C. Sedillo, et al., DNASU plasmid and PSI: Biology-Materials repositories: resources to accelerate biological research, *Nucleic Acids Res.* 42 (2014) D1253–D1260.
- [50] P.K. Smith, R.I. Krohn, G. Hermanson, A. Mallia, F. Gartner, M. Provenzano, et al., Measurement of protein using bicinchoninic acid, *Anal. Biochem.* 150 (1985) 76–85.
- [51] D. Shcherbakov, W. Piendl, A novel view of gel-shifts: analysis of RNA-protein complexes using a two-color fluorescence dye procedure, *Electrophoresis* 28 (2007) 749–755.